Available online at www.sciencedirect.com

SciVerse ScienceDirect

Ceramics International 39 (2013) 6981–6989

CERAMICS INTERNATIONAL

www.elsevier.com/locate/ceramint

Pink ceramic pigments based on chromium doped $M(Al_{2-x}Cr_x)O_4$, M = Mg, Zn, normal spinel

S.R. Prim[b], A. García[a], R. Galindo[a], S. Cerro[a], M. Llusar[a], M.V. Folgueras[b], G. Monrós[a,*]

[a]Department of Inorganic and Organic Chemistry, Jaume I University, Av. de Vicent Sos Baynat, s/n, 12071 Castellón, Spain
[b]Centro de Ciências Tecnológicas, Universidade do Estado de Santa Catarina (UDES), Joinville, Brazil

Received 24 January 2013; received in revised form 13 February 2013; accepted 13 February 2013
Available online 20 February 2013

Abstract

In this paper $M(Al_{2-x}Cr_x)O_4$, M = Mg, Zn and x from 0.05 to 2 compositions, have been prepared by solid state reaction in order to analyse their reactivity, structure, limit of solid solution, stability and pigmenting properties in conventional ceramic glazes. Solid solutions are obtained at 1200 °C in the Zn case (gahnite) and at 1400 °C in the Mg case (magnesium spinel). In both cases powders become pink coloured up to $x=0.4$ and then progressively greenish. Likewise powders glazed in a conventional ceramic glaze matrix of the CaO–ZnO–SiO_2 system for double firing stoneware (1050 °C) produce glazes firstly orange coloured up to $x=0.4$, pink up to $x=1.2$ and finally green at higher x. The colour evolution is associated to the entrance at low doping levels of relatively big Cr^{3+} (0.755 Å) substituting Al^{3+} (0.675 Å) in VI coordinated sites of both spinel lattices; this produces an enhancement of the crystal field strength under the VI coordinated Cr^{3+} that shifts the light absorbances to higher energy and an orange-pink colour can be observed. But when the entrance of Cr^{3+} progresses, the crystal field strength under the ion relaxes and absorption bands shift to higher wavelength when x increases, producing green colours. The UV–vis–NIR spectra of low x pink $M(Al_{2-x}Cr_x)O_4$ compositions are similar to those of ruby $(Cr_{0.1}Al_{1.9})O_3$, indicating analogous mechanism of colour.

Keywords: D. Alkaline earth; D. Perovskites; Ceramic pigment; Chromium

1. Introduction

Red spinel has been considered as a gemstone, but until fairly modern times, all red gemstones were referred to as "rubies" such as the "Black Prince's Ruby" set on the front cross patté of the British Imperial State Crown which has been in the possession of the British kings since it was given in 1367 to its namesake, Edward of Woodstock (the "Black Prince") who received it from Pedro el Cruel, King of Castile, in exchange for the services he had rendered. It was only relatively recently that the rare ruby has been differentiated from the more common spinel that can be distinguished on the basis of hardness and density, namely that a ruby is slightly harder and denser than a spinel but x-ray test is the best method to differentiate between spinel and ruby [1].

Ideal spinel AB_2O_4 can be considered to be built by O^{2-} ions in cubic closed-packed array and A and B ions occupying the interstices in the structure. In the normal structure the A ion occupies one-eighth of the tetrahedral sites and the B ion one-half of the octahedral sites. On the inverse spinel all A ions and one-half of the B ions have exchanged places. Usually the crystal field stabilisation energy (CFSE) of the transition metals present is used to explain the cation distribution on the spinel structure. The preference on the octahedral site is dependent on the d-electron configuration. If the A^{2+} ions have a strong preference for the octahedral site, they will force their way into it and displace half of the B^{3+} ions from the octahedral sites to the tetrahedral sites. If B^{3+} ions have a low or zero octahedral site stabilisation energy (OSSE), then they have no preference and will adopt the tetrahedral site. But this theory cannot explain the marked preference of Al^{3+} (d^0) cations for octahedral sites or of Zn^{2+} (d^{10}) for tetrahedral sites because crystal field theory would predict that both have no site preference. Burdett et al. [2] proposed an alternative

*Corresponding author. Tel.: +34 964 728250; fax: +34 964 728214.
E-mail address: monros@uji.es (G. Monrós).

0272-8842/$ - see front matter © 2013 Elsevier Ltd and Techna Group S.r.l. All rights reserved.
http://dx.doi.org/10.1016/j.ceramint.2013.02.035

treatment of the problem of spinel inversion, using the relative sizes of s and p atomic orbitals of the two types of atoms to determine their site preference, because the dominant stabilizing interaction in solids is not the crystal field stabilisation energy but σ-type interactions between metal cations and oxide anions. Only in cases where this size-based approach indicates no preference for one structure over another do crystal field effects make any difference. The covalence degree of M–O bonds limits also the cation exchange between tetrahedral and octahedral sites as well as the lattice flexibility as described by Ardit et al. in the gahnite–CO–aluminate spinel solid solution [3].

As mentioned above, spinel occurs in almost every colour, and forms gems of all colours, but bright red spinel [4], known as ''Ruby Spinel'', is the most valuable spinel; in the past, there was no distinction between true ruby and spinel, as they look very similar and are found together in the same localities. The spinel gems are based on doping with chromophores (Cr, V, Fe, Mn, etc.) of different compositions: spinel (or magnesium spinel) $MgAl_2O_4$, gahnite (zinc spinel) $ZnAl_2O_4$, hercynite (iron spinel) $FeAl_2O_4$ or galaxite (manganese spinel) $MnAl_2O_4$. In 1960s Arlett [5] studied the crystallisation of chromium-doped magnesium aluminate spinels with varying amounts of excess alumina grown by the flame fusion process. Presumably these crystals contain stoichiometrically significant amounts of defects. When these chromium-doped spinels were annealed at temperatures below their melting

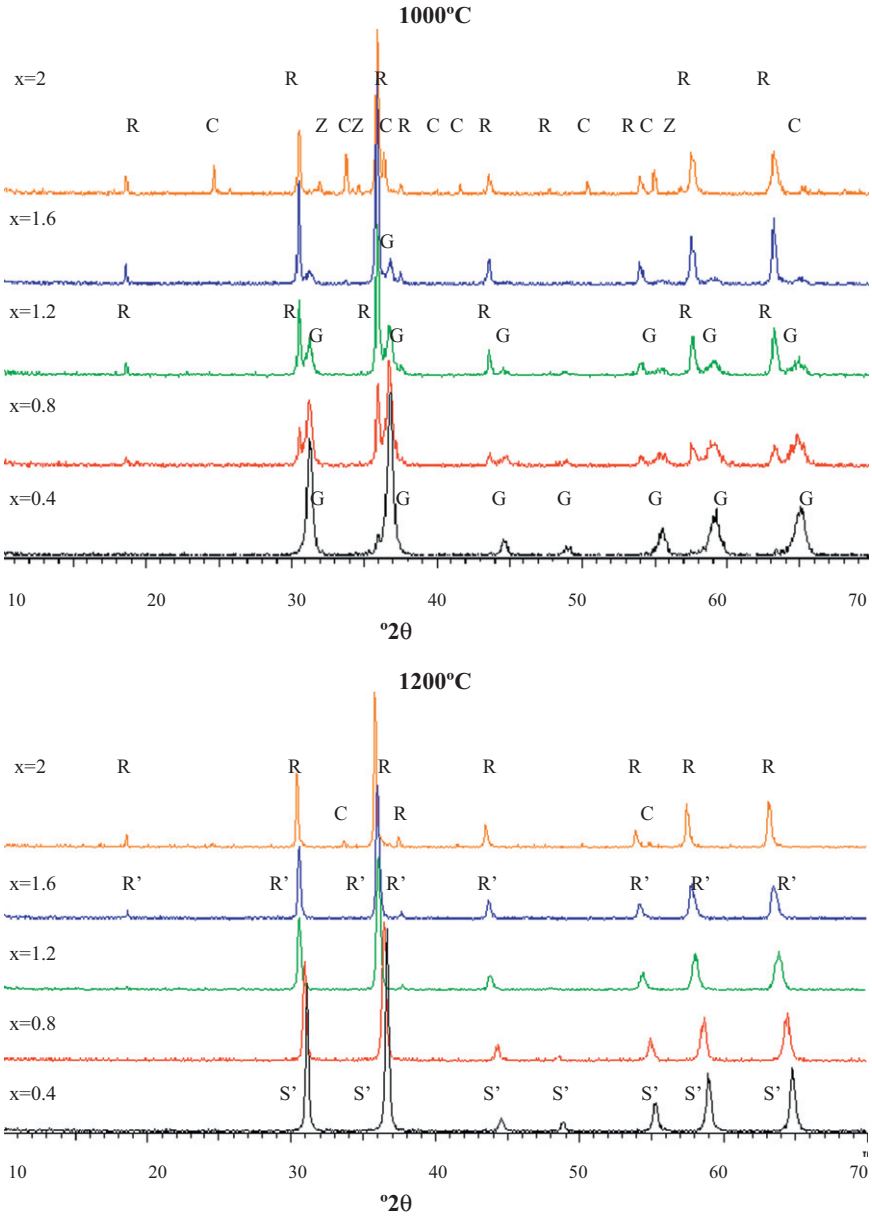

Fig. 1. XRD evolution of $Zn(Al_{2-x}Cr_x)O_4$ fired at 1000 and 1200 °C/3 h. Crystalline phases: G (gahnite $ZnAl_2O_4$), R ($ZnCr_2O_4$), S′ (Cr–$ZnAl_2O_4$ solid solution), R′ (Al–$ZnCr_2O_4$ solid solution), C (eskolaite Cr_2O_3), and Z (ZnO).

point, the spinel structure cannot tolerate such a high concentration of defects and at least some of the excess alumina is exsolved. The chromium ion makes magnesium aluminate spinel pink, whereas in magnesium aluminate spinel containing excess alumina it is green. When exsolution of the alumina occurs during annealing, the aggregate changes to pink.

In this paper $M(Al_{2-x}Cr_x)O_4$, M = Mg, Zn normal spinels with $x=0.05$, 0.1, 0.2, 0.3, 0.4, 0.8, 1.2, 1.6, and 2 compositions, have been prepared by solid state reaction in order to analyse their structural evolution and pigmenting properties in a conventional ceramic glaze matrix of the CaO–ZnO–SiO_2 system for double firing stoneware (1050 °C).

2. Experimental

$M(Al_{2-x}Cr_x)O_4$, M = Mg, Zn normal spinels with $x=0.05$, 0.1, 0.2, 0.3, 0.4, 0.8, 1.2, 1.6, and 2, have been prepared (ceramic route) from magnesium carbonate, zinc oxide, $Al(OH)_3$ and Cr_2O_3 oxide (all supplied by PanreaC S.A.). In the ceramic method the precursors were homogenised in a planetary mill and acetone medium. When acetone was evaporated the raw powders were fired. The sample $x=0.3$ was also prepared adding 0.5 mol/mol of NH_4Cl used as a flux agent. The raw powders were fired successively at 1000 °C, 1200 °C and 1400 °C (for magnesium spinel) with a soaking time of 3 h. Samples have been characterised by several techniques:

a) X-ray diffraction (XRD) carried out on a Siemens D5000 diffractometer using Cu K_α radiation, 20–70° 2θ range, scan rate 0.05° 2θ/s, 2 s per step and 40 kV and 20 mA conditions. Also for measuring parameters of cell unit cell by POWCAL and LSQC programs, XRD difractograms at scan rate 0.01° 2θ/s, 5 s per step and 40 kV and 20 mA conditions were carried out using α-Al_2O_3 as internal standard peaks [6].

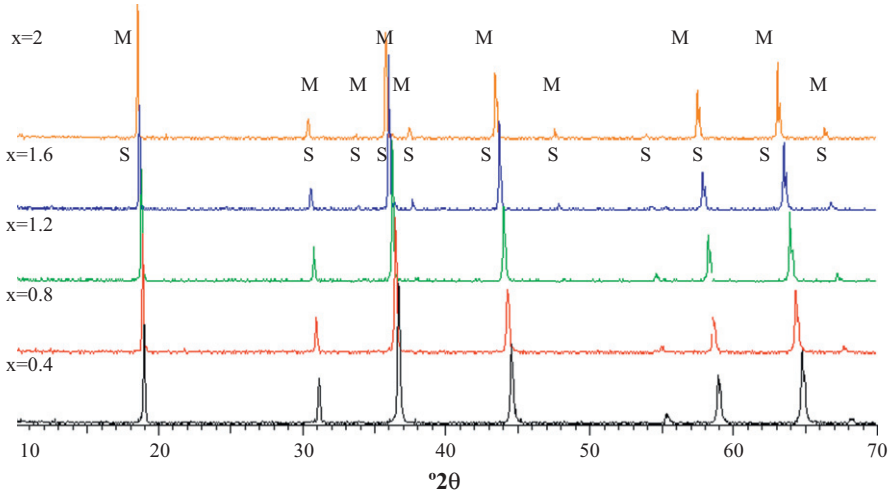

Fig. 2. XRD evolution of Mg $(Al_{2-x}Cr_x)O_4$ fired at 1400 °C/3 h. Crystalline phases: M ($MgCr_2O_4$) and S (Cr–$MgAl_2O_4$ solid solution.

Table 1
XRD evolution with temperature of samples.

		Cr–$ZnAl_2O_4$		Cr–$MgAl_2O_4$		
		1000 °C	1200 °C	1000 °C	1200 °C	1400 °C
x	0.05	G(s)	G(s)			E(S)
	0.1	G(s)	S′(s)			S(s)
	0.2	G(s)	S′(s)			S(s)
	0.3	G(s)	S′(s)	E(m)M(w)P(w)	S(s)P(w)	S(s)
Minute	0.3	G(s)	S′(s)	E(m)M(w)P(vw)	S(s)	S(s)
	0.4	G(s)R(w)	S′(s)			S(s)
	0.8	G(m)R(m)	S′(s)			S(s)
	1.2	G(m)R(s)	R′(s)			S(s)
	1.6	G(w)R(s)	R′(s)			S(s)
	2.0	R(s)C(w)Z(w)	R(s)C(vw)			M(s)

Crystalline phases: E (magnesium spinel $MgAl_2O_4$), M ($MgCr_2O_4$), S (Cr–$MgAl_2O_4$ solid solution), P (periclase MgO), G (Gahnite $ZnAl_2O_4$), R ($ZnCr_2O_4$), S′ (Cr–$ZnAl_2O_4$ solid solution), R′ (Al–$ZnCr_2O_4$ solid solution), C (eskolaite Cr_2O_3), and Z (ZnO). Intensity of peaks: s (strong), m (medium), w (weak), and vw (very weak).

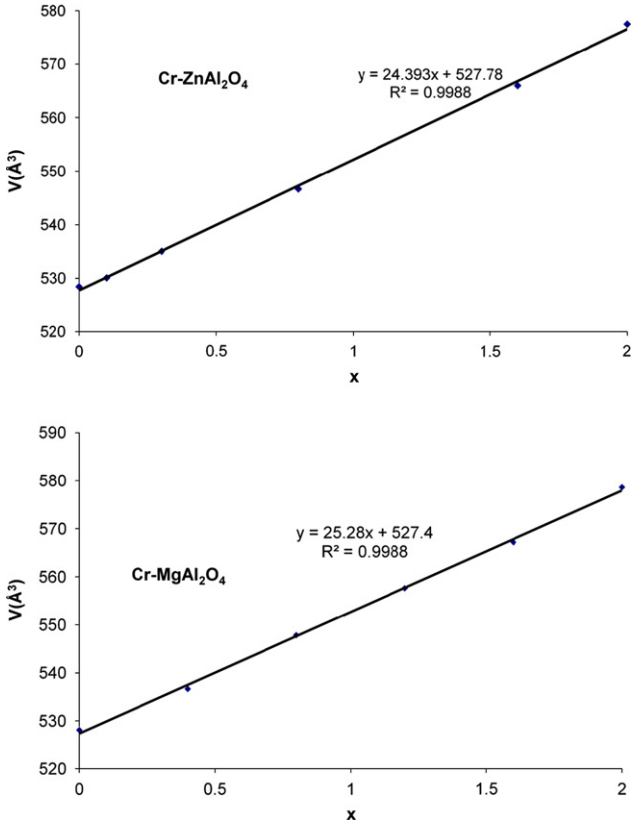

Fig. 3. Evolution of cell volume obtained for $M(Al_{2-x}Cr_x)O_4$, M = Mg, Zn, solid solutions.

b) Microstructure characterisation of powders was carried out by Scanning Electron Microscopy (SEM), using a Leo-440i microscope supplied by LEYCA.
c) UV–vis–NIR spectra of 5% weight glazed samples in a conventional SiO_2–CaO–ZnO glaze for a double firing stoneware (1050 °C) have been collected using a Jasco V670 spectrometer through the diffuse reflectance technique. L^*, a^* and b^* colour parameters of glazed samples were measured following the CIE (Commission International de l'Eclairage) colorimetric method [7] using an X-Rite SP60 spectrometer, with standard lighting D65. In this method, L^* is a measure of brightness (100 = white and 0 = black) and a^* and b^* are of chroma ($-a^*$—green, $+a^*$—red, $-b^*$—blue, and $+b^*$—yellow).

3. Results and discussion

The involved Shannon effective radii [8] of ions B in VI coordination of AB_2O_4 normal spinel are Al^{3+} (0.675 Å) and Cr^{3+} (0.755 Å), and of the ions A in IV coordination are Mg^{2+} (0.80 Å) and Zn^{2+} (0.74 Å): the similarity of size between the ions indicates the possibility of solid solution between them.

XRD difractograms of signified samples and the summary of evolution of crystalline phases detected are shown in Fig. 1 (Cr–$ZnAl_2O_4$), Fig. 2 (Cr–$MgAl_2O_4$) and Table 1. The solid solution of Cr in $Zn(Al_{1-x}Cr_x)_2O_4$ is completed at 1200 °C. Previously at 1000 °C the solid solution of Cr in gahnite $ZnAl_2O_4$ is allowed until $x=0.4$. On the other hand separated crystallisation of gahnite $ZnAl_2O_4$ and chromite of zinc $ZnCr_2O_4$ is detected above $x=0.8$. At 1200 °C the presence, or not, of a peak at 18° 2θ could differentiate the solid solution of chromium in gahnite up to $x=0.8$ (absence) and the solid solution of aluminium in chromite of zinc (presence of the diffraction peak; see Table 1 and Fig. 1). On the other hand the solid solution of Cr in $Mg(Al_{1-x}Cr_x)_2O_4$ is completed at 1400 °C. Previously, at 1200 °C, unreacted periclase MgO was detected together with the solid solution of Cr in spinel $MgAl_2O_4$ and at 1000 °C also magnesiochromite $MgCr_2O_4$ was detected (see Table 1 and Fig. 2). The use of 0.5 mol/mol of NH_4Cl as flux agent for $x=0.3$ samples does not modify the XRD difractogram in the case of $Zn(Al_{1-x}Cr_x)_2O_4$ where both samples (mineralised and unmineralized) allow the solid solution of chromium in gahnite at 1000 °C. But in the case of $Mg(Al_{1-x}Cr_x)_2O_4$ it can be observed that the periclase is not detected in the mineralised sample at 1200 °C, improving the reactivity of the system.

In agreement with the achievement of the solid solution by substitution of a smaller ion Al^{3+} (0.675 Å) for the bigger Cr^{3+} (0.755 Å), lattice parameter measurements, carried out in both $M(Al_{1-x}Cr_x)_2O_4$, M = Mg, Zn spinels (Fig. 3), indicate a gradual increase of the unit cell volume of the spinel with x, following a Vegard linear variation [9].

CIEL*a^* and b^* colour parameters evolutions of the powders and 5 wt% glazed samples in order to evaluate their pigmenting properties in a conventional ceramic glaze matrix of the CaO–ZnO–SiO_2 system for double firing stoneware (1050 °C) are shown in Table 2 and Figs. 4 and 5.

The visual evolution of the powder colour for $Zn(Al_{1-x}Cr_x)_2O_4$ samples at 1200 °C (solid solution completed) starts from a light pink colour ($L^*/a^*/b^* = 86.7/2.8/-0.1$ for $x=0.05$) to progressive increase in a^* (red shade) and decrease in L^* (brightness) up to $x=0.3$ ($L^*/a^*/b^* = 79.1/7.0/0.1$). Nevertheless, from $x=0.4$ a^* diminishes, the powder turns progressively greenish and at $x=1.6$ it is already a green powder. On the other hand, the colour behaviour of glazed samples starts from an orange colour ($L^*/a^*/b^* = 66.0/5.1/18.1$ for $x=0.05$) which progressively increases in a^* (red shade) and decreases in both L^* (brightness) and b^* (yellow shade) up to $x=0.4$ ($L^*/a^*/b^* = 79.1/7.0/0.1$), but from $x=0.4$ a^* diminishes slightly but b^* diminishes dramatically (see Fig. 4). The resulting colour becomes pink for $x=0.8$ ($L^*/a^*/b^* = 55.5/5.6/9.7$), then greenish gradually and $x=1.6$ is already green ($L^*/a^*/b^* = 46.5/-4.7/9.7$).

The evolution of the colour for $Mg(Al_{1-x}Cr_x)_2O_4$ samples at 1400 °C (solid solution completed) is very similar to the above discussed $Zn(Al_{1-x}Cr_x)_2O_4$ samples. The powder colour starts from a light pink colour that progressively increase in intensity up to $x=0.4$ ($L^*/a^*/b^* = 75.7/4.8/2.7$),

Table 2
CIE $L^*a^*b^*$ parameters evolution with temperature of samples.

Sample	$Cr–ZnAl_2O_4$		$Cr–MgAl_2O_4$		
	1000 °C	1200 °C	1000 °C	1200 °C	1400 °C
$x=0.05$					
Powder	87.7/0.9/5.0	86.7/2.8/−0.1	87.8/−2.6/11.9	87.5/0.6/2.1	
Glazed	64.3/4.7/17.5	66.0/5.1/18.1	65.2/3.5/20.0	67.9/4.1/17.9	
$x=0.1$					
Powder	85.4/1.8/5.8	86.7/4.3/0.6	84.2/−2.3/11.3	84.7/1.4/2.4	
Glazed	63.0/6.4/18.0	62.0/5.2/16.1	64.5/2.3/ 18.6	60.3/5.5/16.4	
$x=0.2$					
Powder	82.1/3.5/5.1	82.9/6.1/0.1	77.4/−1.9/9.9	82.5/1.5/2.1	
Glazed	59.4/4.7/13.8	59.4/6.3/16.7	58.8/3.0/16.6	60.1/4.1/15.9	
$x=0.3$					
Powder	79.7/3.8/3.9	79.1/7.0/0.1	75.8/−1.4/9.1	78.6/2.0/1.6	
Glazed	56.9/3.6/11.8	55.0/6.8/15.1	56.2/2.6/15.9	58.2/4.0/16.1	
0.3 min					
Powder	79.5/4.7/2.3	77.4/6.1/0.3	76.6/0.5/ 5.9	80.5/3.7/1.2	
Glazed	56.5/4.7/12.5	55.3/6.9/14.9	52.4/3.7/12.9	58.6/4.8/17.5	
0.4 min					
Powder	77.6/1.9/4.4	79.3/5.3/−0.1			75.7/4.8/2.7
Glazed	55.8/ 5.1/15.6	54.6/7.7/16.6			56.5/8.4/14.7
0.8 min					
Powder	73.8/−1.5/ 5.1	74.3/3.8/2.5			70.3/2.8/5.5
Glazed	53.8/−3.6/11	55.5/5.6/9.7			53.3/5.1/ 8.1
1.2 min					
Powder	69.2/−5.0/7.2	68.0/0.6/5.9			64.3/−1.6/7.8
Glazed	50.7/−7.4/11.2	53.1/2.8/9.6			48.5/−1.1/9.7
1.6 min					
Powder	57.0/−2.2/ 8.6	59.1/−4.6/7.9			57.2/−6.7/8.9
Glazed	44.0/−3.8/10.3	46.5/−4.7/9.7			43.4/−6.7/10
2.0 min					
Powder	40.1/1.7/6.3	44.6/−1.7/8.1			48/−10.8/9.2
Glazed	27.9/−1.1/6.6	36.1/−3.3/6.7			41.3/−11/10.4

but from $x=0.4$ a^* diminishes and the powder progressively turns greenish and at $x=1.2$ is green coloured ($L^*/a^*/b^*=64.3/-1.6/7.8$). The colour behaviour of glazed samples starts from an orange colour up to $x=0.4$ ($L^*/a^*/b^*=56.5/8.4/14.7$), but as in the case of $Cr–ZnAl_2O_4$ solid solutions, from $x=0.4$ a^* diminishes slightly but b^* diminishes dramatically (see Fig. 5), and the colour becomes pink for $x=0.8$ ($L^*a^*b_*=53.3/5.1/8.1$), then greenish and at $x=1.2$ it is green ($L^*/a^*/b^*=48.5/-1.1/9.7$).

The evolution of a^* and b^* parameters of both powder and glazed samples are shown in Figs. 4 and 5 goes from orange shade (a^* and b^* relatively high but b^* double of a*, at low x), to pink at middle x (a^* and b^* relatively high but with similar values) and green at high x (a^* negative).

UV–vis–NIR spectra of powders and glazed samples are shown in Figs. 6 and 7. They show two bands at 250–280 and 350–380 nm in the UV range, two broad bands at 420–465 and 570–600 nm and a double hump at 660–710 nm in the visible range. All these bands can be associated to transitions of Cr^{3+} in octahedral coordination [10–12]: (a) three main parity-forbidden transitions $^4A_2(^4F)\rightarrow{}^4T_2(^4F)$ at 570($\pm$10) nm and $^4A_2(^4F)\rightarrow{}^4T_1(^4F)$ at 445($\pm$10) nm, which overlap, and $^4A_2(^4F)\rightarrow{}^4T_2(^4P)$ at 235($\pm$10) nm which overlaps with $Cr^{3+}\leftrightarrow O^{2-}$ band transfer, (b) two weak Cr^{3+} spin-forbidden transitions ($^4A_2(^4F)\rightarrow{}^2T_1(^2G)$ and $^4A_2(^4F)\rightarrow{}^2E(^2G)$ that overlap in the 735–740($\pm$10) nm range. The band assignation for UV–vis–NIR of glazed samples is shown in Table 3.

The UV–vis-NIR spectra of solid solutions in Figs. 6 and 7 and Table 3 shift to higher wavelength (lower energy) when x increases. The entrance at low doping levels of relatively big Cr^{3+} (0.755 Å) substituting Al^{3+} (0.675 Å) in VI coordinated sites of both spinel lattices produces an enhancement of the crystal field strength under the VI coordinated Cr^{3+} that shifts the absorbances to higher energy (lower wavelength). However when the entrance of Cr^{3+} progresses the crystal field strength under the ion relaxes and bands absorption shifts to lower energy (higher wavelength) when x increases. The UV–vis–NIR spectra evolution of a green ($L^*/a^*/b^*=66/-9/15.4$) glazed sample with 5 wt% of eskolaite (Cr_2O_3) is shown in Fig. 8a, and for a ruby ($L^*/a^*/b^*=68.7/6.2/14.8$) glazed sample with 5 wt% of chromium doped corundum ($(Cr_{0.1}Al_{1.9})O_3$, obtained by solid state reaction from

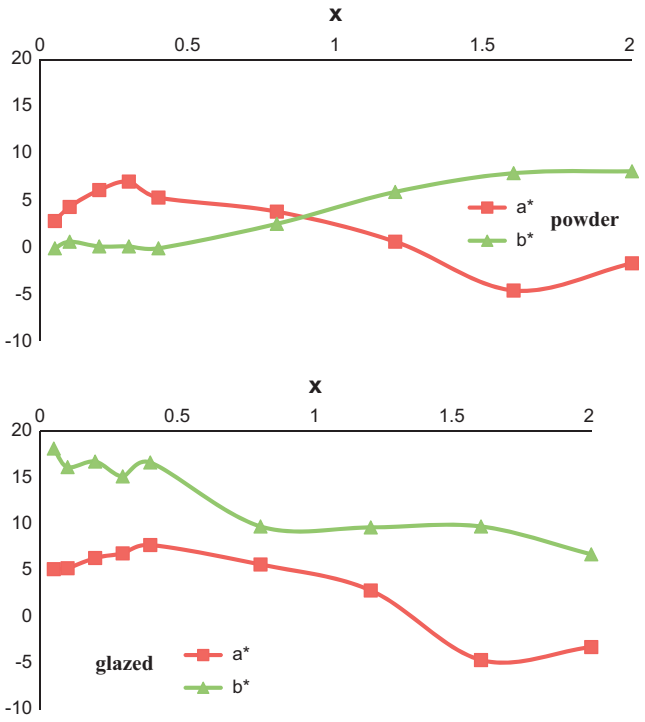

Fig. 4. Evolution of a^* and b^* colour parameters of $Zn(Al_{2-x}Cr_x)O_4$ samples fired at 1200 °C/3 h.

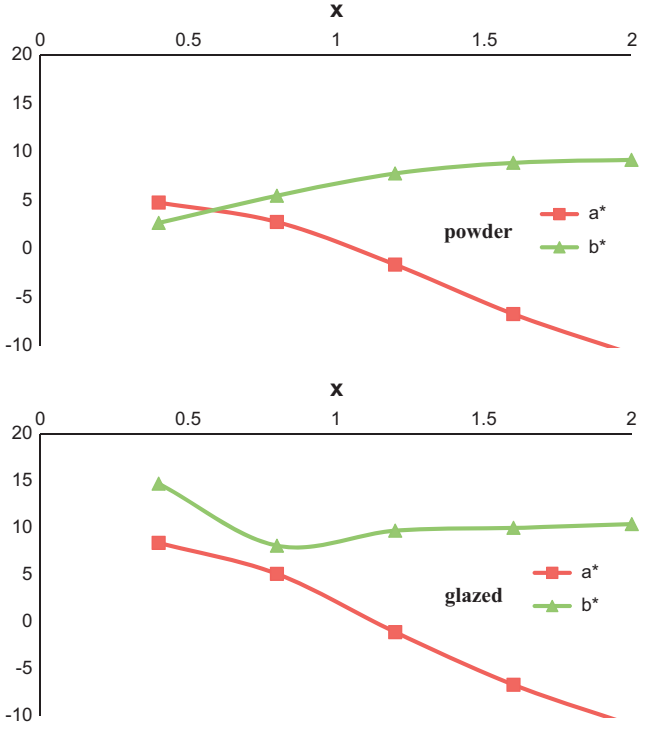

Fig. 5. Evolution of a^* and b^* colour parameters of $Mg(Al_{2-x}Cr_x)O_4$ samples fired at 1400 °C/3 h.

aluminium hydroxide and eskolaite as precursors fired at 1100 °C/2 h, is shown in Fig. 8b. UV–vis–NIR band localisation and assignment are shown in Table 3. Racah

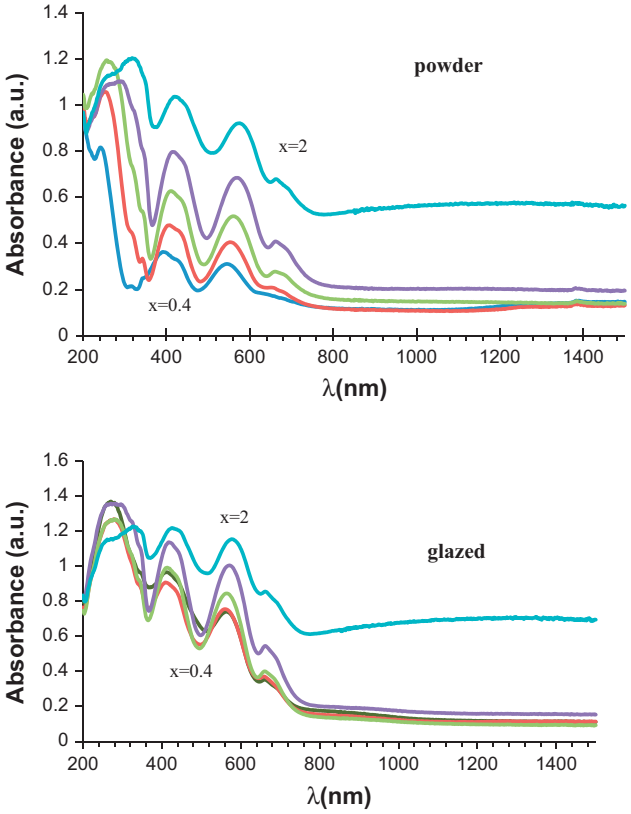

Fig. 6. UV–vis–NIR spectra evolution of $Zn(Al_{2-x}Cr_x)O_4$ samples fired at 1200 °C/3 h.

(B) and nefelauxetic parameters ($\beta = B/B'$ where $B' = 918$ cm^{-1} is the Racah for free ion) of glazed samples, obtained by Tanabe–Sugano diagrams, are also shown in Table 3 [3,12,13]. It can be observed that the spectra features of $M(Al_{1-x}Cr_x)_2O_4$ and $(Cr_{0.1}Al_{1.9})O_3$ are similar: the undoped corundum shows the lowest nefelauxetic β parameter (0.54) similar to the green shade Cr–spinel solid solutions (0.59); likewise, the pink Cr–Al_2O_3 and pink Cr–spinel show similar and higher β parameter (around 0.64), indication of low covalent character in the bond of these pink samples.

The microstructure of representative powders observed by SEM is shown in Fig. 9. In all cases aggregates of particles can be observed. In the case of pink powders ($x = 0.4$ for $Zn(Al_{2-x}Cr_x)O_4$ and $Mg(Al_{2-x}Cr_x)O_4$ in Fig. 9) the fine aggregates (about 2 μm of size for $Zn(Al_{2-x}Cr_x)O_4$ and $Mg(Al_{2-x}Cr_x)$) are integrated by 2–3 particles of 0.5–1 μm diameter which shows an irregular shape. When x increases the sizes of particles and aggregates increases and particles show a regular cubic shape. For green coloured samples, cubes of 1 μm of size forming aggregates of 3–6 μm can be observed for $x = 2$ $Zn(Al_{2-x}Cr_x)O_4$ and cubes of 2 μm of size forming aggregates of 10 μm can be observed for $x = 2$ $Mg(Al_{2-x}Cr_x)O_4$ (see Fig. 9). $Mg(Al_{2-x}Cr_x)O_4$ samples show both larger particle and aggregate size than those of Zn samples.

4. Conclusions

Solid solutions $M(Al_{2-x}Cr_x)O_4$, M = Mg, Zn, normal spinels have been prepared by solid state reaction at 1200 °C in the Zn case (gahnite) and at 1400 °C in the Mg case (magnesium spinel). In both cases powders become pink coloured until $x = 0.4$ and then progressively greenish. Likewise when powders pigmenting properties are checked in a conventional ceramic glaze matrix of the $CaO–ZnO–SiO_2$ system for double firing stoneware (1050 °C), the glazes become firstly orange coloured up to $x = 0.4$, pink up to $x = 1.2$ and finally green at higher x. The colour evolution is associated to the entrance at low doping levels of the relatively bigger Cr^{3+} (0.755 Å) substituting Al^{3+} (0.675 Å) in VI coordinated sites of both spinel lattices; this produces an enhancement of the crystal field strength under the VI coordinated Cr^{3+} that shifts its light absorbances to higher energy (lower wavelength) and an orange-pink colour can be observed. Nevertheless, as the entrance of Cr^{3+} progresses the crystal field strength under the ion relaxes and bands absorption shifts to lower energy (higher wavelength) when x increases, and then gives green colours. The UV–vis–NIR spectra features of $M(Al_{1-x}Cr_x)_2O_4$ and ruby $(Cr_{0.1}Al_{1.9})O_3$ are similar: The undoped corundum shows the lowest nefelauxetic β parameter (0.54) similar to those of the green shade Cr–spinel solid solutions (0.59), likewise, the pink $Cr–Al_2O_3$ and pink Cr–Spinel show similar and higher β parameter (around 0.64), indication of low covalent character in the bond for these pink samples and an analogous mechanism of colour in both cases.

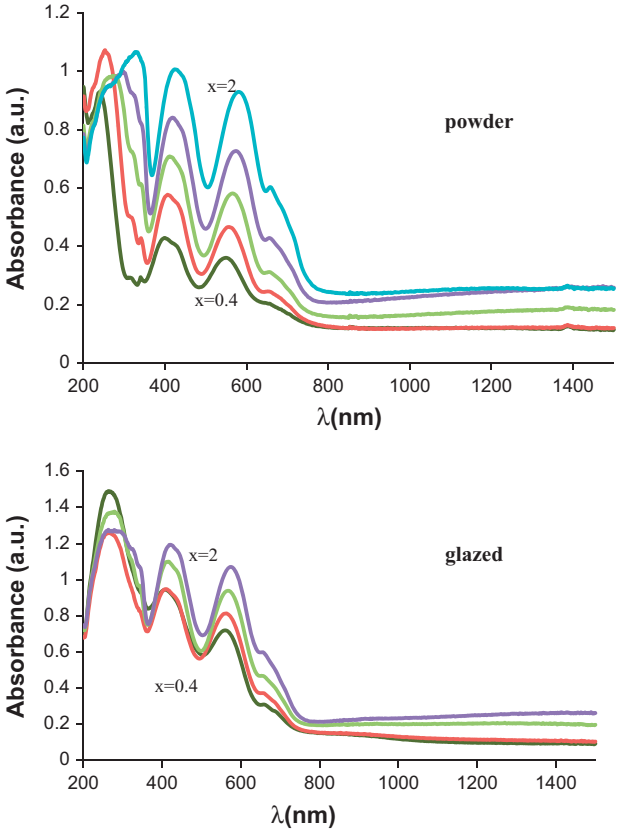

Fig. 7. UV–vis–NIR spectra evolution of $Mg(Al_{2-x}Cr_x)O_4$ samples fired at 1400 °C/3 h.

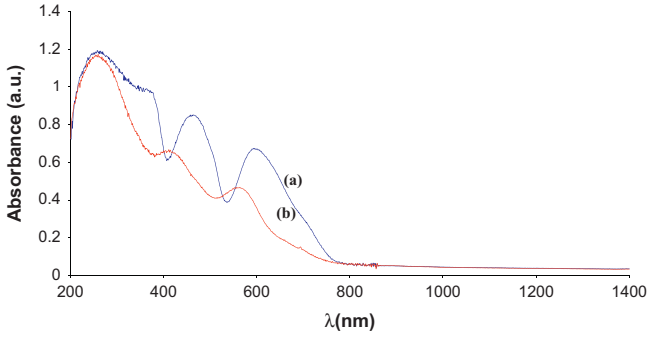

Fig. 8. UV–vis–NIR spectra evolution of: (a) green ($L^*/a^*/b^* = 66/-9/15.4$) glazed sample with 5 wt% of eskolaite (Cr_2O_3) and (b) ruby ($L^*/a^*/b^* = 68.7/6.2/14.8$) glazed sample with 5 wt% of chromium doped corundum $(Cr_{0.1}Al_{1.9})O_3$.

Table 3
Band assignation for UV–vis–NIR, Racah (B) and nefelauxetic (β) parameters of glazed samples obtained by Tanabe–Sugano diagrams.

	$Cr–ZnAl_2O_4$ (1200 °C)			$Cr–MgAl_2O_4$ (1400 °C)			Cr_2O_3	$(Cr_{0.1}Al_{1.9})O_3$
	$x=0.4$ orange	$x=0.8$ pink	$x=2$ green	$x=0.4$ orange	$x=0.8$ pink	$x=2$ green	green	pink
$^4A_2(^4F) \rightarrow {}^4T_2(^4F)$ at 570(±10) nm	570	570	590	560	560	570	600	564
$^4A_2(^4F) \rightarrow {}^4T_1(^4F)$ at 445 nm	420	420	440	410	410	430	465	415
$^4A_2(^4F) \rightarrow {}^4T_2(^4P)$ at 235 nm	260/380	260/380	260/380	250/380	250/380	250/360	250/350	265
$(^4A_2(^4F) \rightarrow {}^2T_1(^2G)$ 735–740 nm	660	660	670	660	660	660	710	–
$^4A_2(^4F) \rightarrow {}^2E(^2G)$ 735–740 nm	690	690	700	–	–	–	–	–
B′ (cm^{-1})	582.5	582.5	536.9	610.6	610.6	544	495	582.5
β	0.64	0.64	0.59	0.65	0.65	0.59	0.54	0.64
Δ_0 (cm^{-1})	18,465	18,465	17,449	18,684	18,864	17,843	16,781	18,684

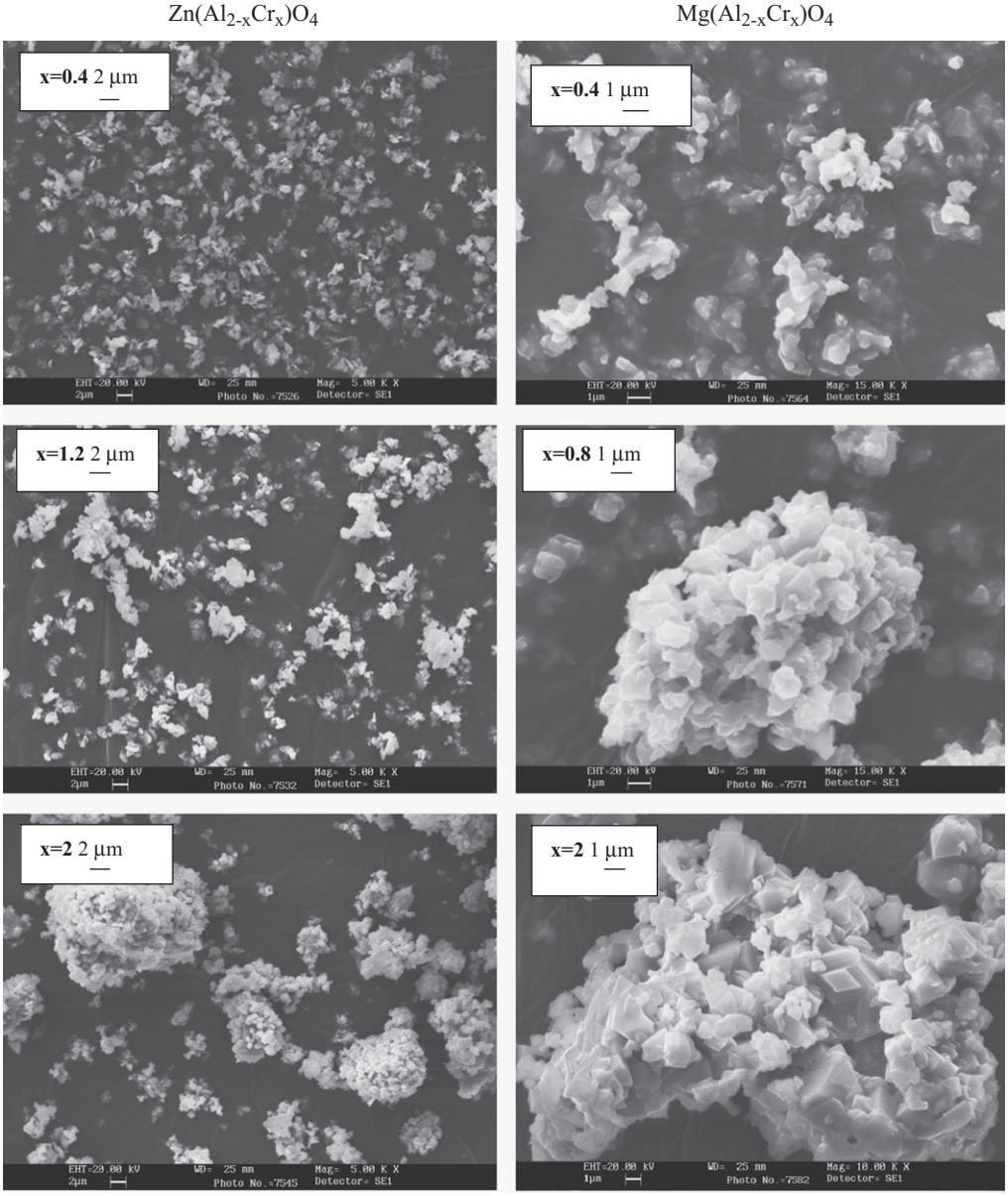

Fig. 9. SEM micrographs of representative powders.

Acknowledgements

Authors acknowledge the financial support given by Fundación Caja Castellón-UJI, P1-1B2010-09 Project. S.R. Prim acknowledges grant funding from Brazilian CAPES.

References

[1] D. Hoak Dale, The Iconography of the Crown Imperial, Tudor Political Culture, Cambridge University Press, Cambridge, 2002.
[2] J.K. Burdett, G.L. Price, S.L. Price, Role of the crystal-field theory in determining the structures of spinels, Journal of the American Chemical Society 104 (1982) 92–95.
[3] M. Ardit, G. Cruciiani, M. Dondi, Structural relaxation in tetrahedrally coordinated Co^{2+} along the gahnite–Co–aluminate spinel solid solution, American Mineralogist 97 (2012) 1394 140.
[4] P.G. Read, In Gemmology, third ed., Elsevier, Oxford, 2005, p. 289.
[5] R.H. Arlett, Behavior of Chromium in the System $MgA_{12}O_4$–$A_{12}O_3$, Journal of the American Ceramic Society 45 (1962) 523–527.
[6] POWCAL and LSQC programmes, Department of Chemistry, University of Aberdeen, UK.
[7] C.I.E. Comission International de l'Eclairage, Recommendations on Uniform Colour Spaces, Colour Difference Equations, Psychometrics Colour Terms. Supplement No. 2 of CIE Pub. No. 15 (E1-1.31), 1971, Bureau Central de la CIE, Paris, 1978.
[8] R.D. Shannon, Revised effective ionic radii and systematic studies of interatomic distances in halides and chalcogenides, Acta Crystallographica A32 (1976) 751–767.
[9] L. Vegard, Die Konstitution der Mischkristalle und die Raumfüllung der Atome, Zeitschrift für Physik 5 (1921) 17–22.
[10] G. Monrós, H. Pinto, J. Badenes, M. Llusar, M.A. Tena, Chromium(IV) stabilisation in new ceramic matrices by coprecipitation

method: application as ceramic pigments, Zeitschrift für Anorganische und Allgemeine Chemie 631 (2005) 2131–2135.

[11] S. Ishida, M. Hayashi, Y. Fujimura, K. Fujiyoshi, Spectroscopic study of the chemical state and coloration of chromium in rutile, Journal of the American Ceramic Society 73 (11) (1990) 3351–3355.

[12] A.B. Lever, Studies in Physical and Theoretical Chemistry, Inorganic Electronic Spectroscopy, vol. 3, Elsevier, Amsterdam, 1986.

[13] Y. Tanabe, S. Sugano, On the absorption spectra of complex ions III, Journal of the Physical Society of Japan 11 (8) (1956) 864–877.